Strain hardening behaviour of a Nickel based superalloy SUPERCAST 247A

Avala Lavakumar, Ch.V.S.Murthy, D.V.V.Satyanarayana, and N.Eswara prasad

Abstract— Experimental true stress – true strain data of the alloy Supercast 247A in as-cast as well as different heat treated conditions have been analyzed using different flow relationships. Ludwigson relationship provides the best fit of the data for all the conditions. The flow data of the alloy in all conditions, fitted according to Ludwigson model not only yields a unique set of flow parameters for each ageing condition but also exhibit a systematic trend. The alloy in all heat treatment conditions exhibit two distinct stages of strain hardening with strain hardening rate decreasing rapidly in regime I and remaining essentially constant in regime II. The alloy subjected to solution treatment followed by single step ageing exhibits finer γ' structure and thereby the highest strain hardening rate of all the conditions studied. The strain hardening rate of the alloy progressively decreases as the size of γ' increases from solutionising + single aged condition through solutionising + double aged and as-cast conditions to as-cast plus direct aged condition.

Index Terms— Supercast 247A, Solutionising, Ageing, Strain hardening, Deformation, Flow behavior, superalloy.

1 INTRODUCTION

THE flow curve signifies macroscopic plastic deformation behavior under a definite structure, state and deformation condition. Several flow relationships such as Hollomon, Ludwik, Voce, Swift and Ludwigson have been proposed in the past in order to establish an analytical relation between true stress (flow stress, σ) and true strain (ε) [1-5]. Yet, description of plastic flow behavior of several metals and alloys is frequently carried out using either the Hollomon relationship ($\sigma = K_H \varepsilon^{n_H}$) or the Ludwik relationship ($\sigma = \sigma_0 + K_L \varepsilon^{n_L}$). Ludwigson [5] has demonstrated that the flow behavior of face centered cubic (FCC) metals and alloys having low stacking fault energy, could not, however, be adequately described either by the Hollomon or Ludwik equation and hence an alternative relationship has been suggested, which is given by

$$\sigma = K_1 \varepsilon^{n_1} + exp\left(K_2 + n_2 \varepsilon_p\right) \qquad (1)$$

where σ is the true stress, ε_p the true plastic strain, K_1 and n_1 are the strength coefficient and strain hardening exponent respectively, and K_2 and n_2 have been introduced as additional constants. It was suggested that the additional term $exp\left(K_2 + n_2 \varepsilon_p\right)$ in equation (1) accounts for the deviation from the Hollomon equation at lower strain levels.

Furthermore, characterization of the strain hardening behavior is an important first step in microstructural investigation of plastic deformation in the material as it often provides clear indications of the onset of many of the microstructural changes occurring during deformation [5-17]. The strain hardening behavior of both stable and unstable austenitic stainless steels(ASSs) has been investigated in the past [5-11]. It has been established that the deformation modes that control the rate of strain hardening during cold working in commercial ASS grades is dependent on composition and the temperature of deformation. In unstable ASS grades such as AISI 301 (17Cr-7Ni), and 304 (17Cr-9Ni), the strain induced martensite formation takes place at relatively higher strain hardening rate [9]. On the other hand, in stable ASS grades like AISI 316 (17Cr-11Ni) and 310 (25Cr-20Ni), the rate of strain hardening is dictated solely by stacking fault energy (SFE), which in turn depends on the alloy composition [7].

In case of precipitation hardened alloys such as iron- and nickel- based superalloys, the strain hardening behavior is dictated by size and nature of precipitates and in turn by a particular dislocation bypass mechanism [12-14]. Del Valle et al. [13] have investigated the effect of γ' structure on plastic deformation behavior during stage II of work hardening in Nickel base superalloy Inconel X 750. It has been reported that the effect of γ' size on stage II work hardening rate is dependent on nature of dislocation-precipitate interaction. Their study has revealed that when γ' size is greater than about 50 nm, Orowan looping is the bypass mechanism and under such conditions strain hardening rate is found to decrease with increasing γ' size. On the other hand, when γ' size is less than about 50 nm, precipitate shearing is the controlling mechanism and strain hardening rate is found to decrease with decreasing γ' size.

The Supercast 247A alloy considered for the present investigation is a cast nickel base superalloy and derives its strength from precipitation of fine coherent γ' within FCC γ matrix. Supercast 247A is widely used as gas turbine blades and vanes in both military and civil aircrafts due to its excellent creep and stress rupture properties. The present study is aimed at identifying an appropriate flow equation that provides the best fit of true stress-true plastic strain data of the alloy in different microstructural conditions (i.e., as cast as well as different heat treatment conditions) and investigating the strain hardening behavior.

- *A.LavaKumar Assistant professor, Maulana Azad National Institute of Technology Bhopal, India. E-mail: lavakumar.manitb@yahoo.in*
- *Ch.V.S Murthy and N Eswaraprasad Scientists in RCMA (Materials), Hyderabad, India.*
- *D.V.V.Satyanarayana, Scientist, Defence Research Metallurgical laboratory Hyderabad, India.*

2 Experimental Procedure

Nickel base superalloy Supercast 247A was melted at Mishra Dhatu Nigam (MIDHANI), Hyderabad, India and the nominal composition of the alloy in wt % is C-0.074, Cr-8.2, Co-9.3, Mo-0.5, Ta-3.2, Ti-0.8, W-9.5, Al-5.6, Hf-1.5, B-0.015, Zr-0.014 and balance – Ni. The alloy in remelt stock form with poly crystalline microstructure was used in the present study. The test bars of 12mm diameter were given three different heat treatments viz., direct ageing, solutionising plus aging and solutionising plus double ageing. The details of the heat treatment schedules are given in Table 1. Detailed microstructural examination of the alloy in different heat treatment conditions was carried out using optical and scanning electron microscopy. Tensile tests at room temperature were conducted on Instron 5500R universal testing machine at a crosshead speed of 1 mm/ min (i.e., at an initial strain rate of ~$5X10^{-4}$ s^{-1}) using round specimens of gauge length 25 mm and diameter 3.88 mm. The axial strain was monitored with the help of an extensometer of 25 mm gauge length span.

TABLE1

Heat treatments given to the as-received (as cast) bars

Condition	Heat Treatment cycle
As cast (I)	--------
Direct ageing(II)	870^{0}C/20Hrs → Air cooling (AC) to Room temperature (RT)
Solutionising + Single ageing (III)	Solutionising at 1230^{0}C/2hrs + 1260^{0}C/2hrs → AC to RT + Ageing at 870^{0}C/20hrs → AC to RT
Solutionising + double ageing (IV)	Solutionising at 1230^{0}C/2hrs + 1260^{0}C/2hrs+ 1080^{0}C/4hrs→AC to RT + Ageing at 870^{0}C/20hrs →AC to RT

3 Results and Discussion

3.1 True stress –True strain behavior

Figure 1 shows the true stress versus true plastic strain plots of the Supercast 247A alloy at 298K, in all the conditions on log-log scale. Considerable increase in flow stress following full heat treatment involving solution treatment and ageing can be noted from Fig.1. However, the flow stress, subsequently, decreases with double ageing. Furthermore, the experimental σ-ε data for all the conditions, on log-log scale exhibit two slope behavior with a gradual transition. In addition, the transition strain was found to vary with conditions. Alloy in as cast and as cast plus direct ageing condition exhibit almost in same level of flow stress.

Figure 2 illustrates the results of the fit of various flow relationships given in Table 2 for all the conditions. Typical χ^2 (where χ^2 is the sum of residual squares of a fit) values for the

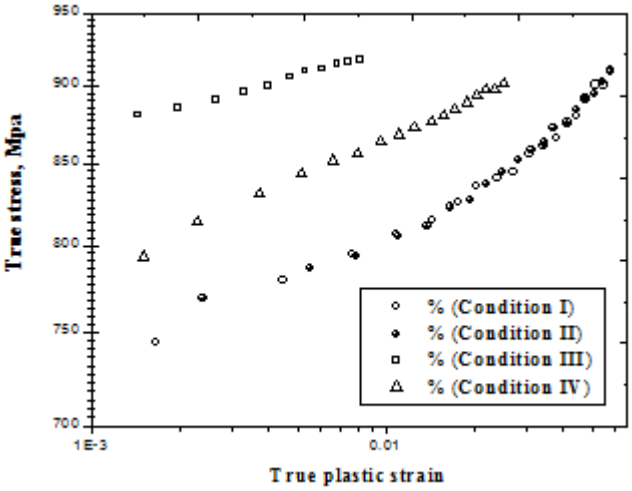

Fig.1 True stress-true plastic strain curves of Supercast 247A alloy in as cast and different heat treatment conditions

above relationships for the complete range of fit of σ-ε data are given in Table 3. As evident from Fig.1, the log-log plots of true stress-true plastic strain are linear at high strains, suggesting the applicability of the Hollomon equation only at high strains i.e., above transition strain. In these figures, an average line for the complete range of σ-ε data shows large deviation from the Hollomon equation leading to a large underestimation of stress values at very low and high strains, while, overestimation at intermediate stresses. Thus, the observed behavior suggests the incapability of the Hollomon equation for the complete range of experimental σ-ε data. This is reflected in the high χ^2 values (Table 2) obtained for different microstructural conditions at 298K.

Of the three flow relationships (Hollomon, Ludwik and Ludwigson), the Ludwigson relationship provides the best fit of the σ-ε data for all the conditions. This is substantiated by the lowest χ^2 values obtained in this case of Ludwigson equation compared to those obtained for other relationships. On the other hand, Ludwik relationship provides better fit of the data at higher strain levels but poor fit at lower strain levels.

Table 2. Value of χ^2 obtained with different flow relationships using experimental true stress – true plastic strain data of Supercast 247A alloy bars, obtained at room temperature (298 K)

Heat Treatment	Hollomon	Ludwik	Ludwigson
As cast	91.328	18.598	8.736
Direct ageing	118.739	2.808	3.778
Solutionising + single ageing	9.140	6.969	4.603
Solutionising + double ageing	8.666	4.789	1.353

Table 3. Summary of flow curve parameters (in Ludwigson equation) of Supercast 247A alloy bars for different heat treatment and as cast conditions, obtained at room temperature (298 K)

Heat Treatment	K_1(Mpa)	n_1	K_2	n_2	ε_L
As cast	1202	0.10	5.04	-99.7	0.024
Direct ageing	1122	0.08	3.87	-153.43	0.016
Solutionising + single ageing	1180	0.03	4.76	-266.59	0.08
Solutionising + double ageing	1072	0.048	3.59	-165.59	0.010

Thus as evident from Fig. 2 and, also the values of χ^2 (Table 2) indicate, the Ludwigson relationship provides the best fit of the experimental σ-ε data of the alloy in different heat treatment and as cast conditions studied at 298 K. The ability of Ludwigson equation for the best description of the flow behavior, as pointed out by the earlier investigation [6,10], can possibly be attributed to larger number of parameters in the equation as compared to other relationships (which have either two or three parameters). This is because the larger the number of parameters in an equation, the closer will be its approximation to the experimental data.

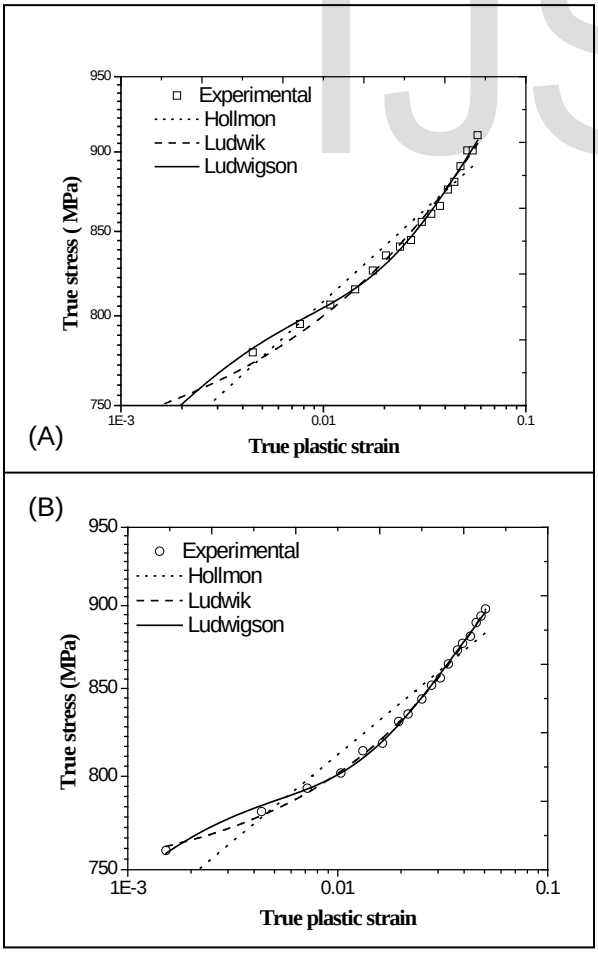

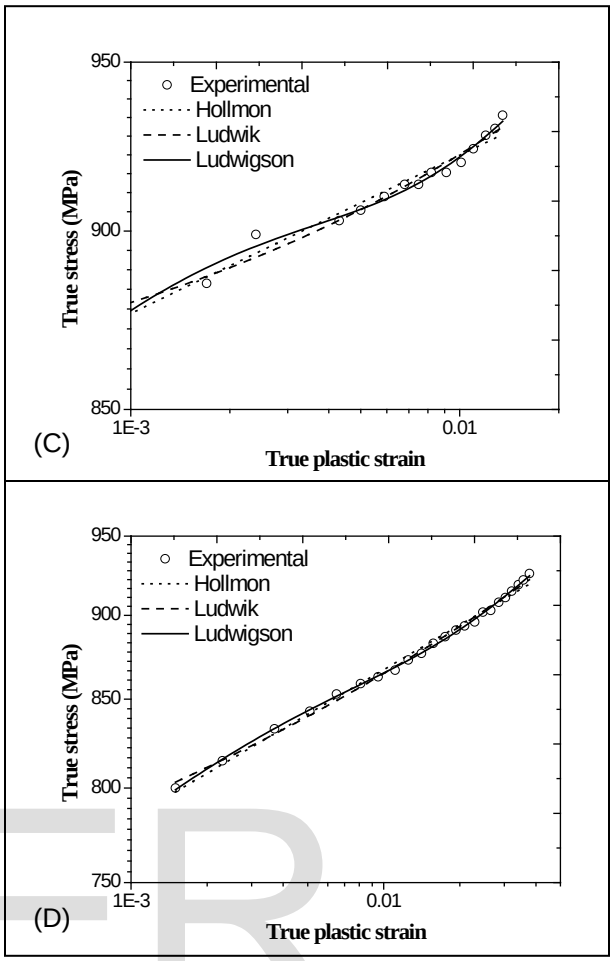

Fig. 2 True stress-True plastic strain data of Supercast 247A alloy at 298 K, fitted using various flow relationships (A) As cast (B) As cast + Ageing (C) Sol. + Ageing (D) Sol. + Double ageing.

However, it is important to consider the physical significance of the parameters before selecting any empirical equation to fit the data. The advantage of using the Ludwigson equation [5] is that it not only accounts for transient flow at low strains but also provides basis for correlation of flow parameters with microstructural parameters (such as precipitate size) and associated substructural changes. Since the Ludwigson relationship has provided the best fit of the experimental data (Table 2) for all the conditions studied, further analysis is confined to this relationship.

Following the method of Ludwigson [5], various flow parameters were determined. The parameters K_1 and n_1 were determined using high strain range (HSR) data plotted in terms of log (σ) versus log (ε) in Fig. 5 (a). Constants n_2 and K_2 were determined from the low strain range (LSR) data plotted in terms of ln (Δ) versus true plastic strain, as shown in Figs. 5 (b). Here 'Δ' is the difference between the observed true stress at low strain and the true stress represented by the linear portion (Hollomon relation) extended to low strains (Fig.3). Following Ludwigson [5], the transition strain, ε_L above which the Hollomon relation represents the HSR data was also de-

termined. Various flow curve parameters thus obtained were used in fitting the Ludwigson equation to the experimental σ-ε data (Fig. 3). The best fit, as indicated by the χ^2 value, was obtained through iteration. The constants thus resulted from the best fit were finally considered and reported in Table 3.

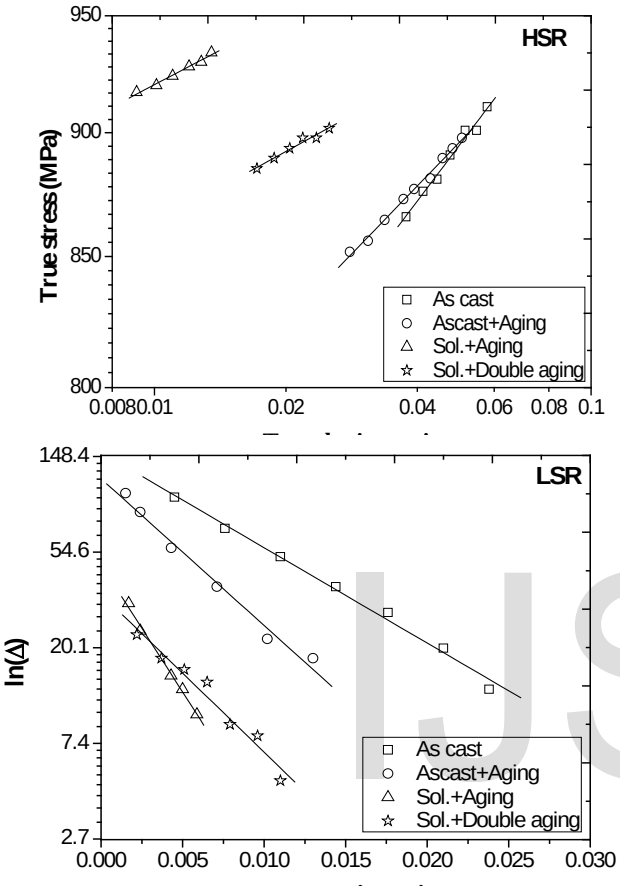

Fig. 3. Determination of flow parameters (a) K_1 and n_1 and (b) K_2 and n_2 of the Supercast 247A alloy bar following the method of Ludwigson.

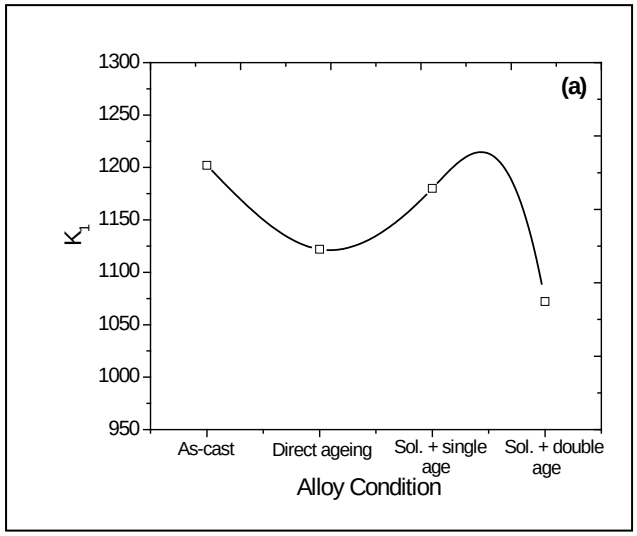

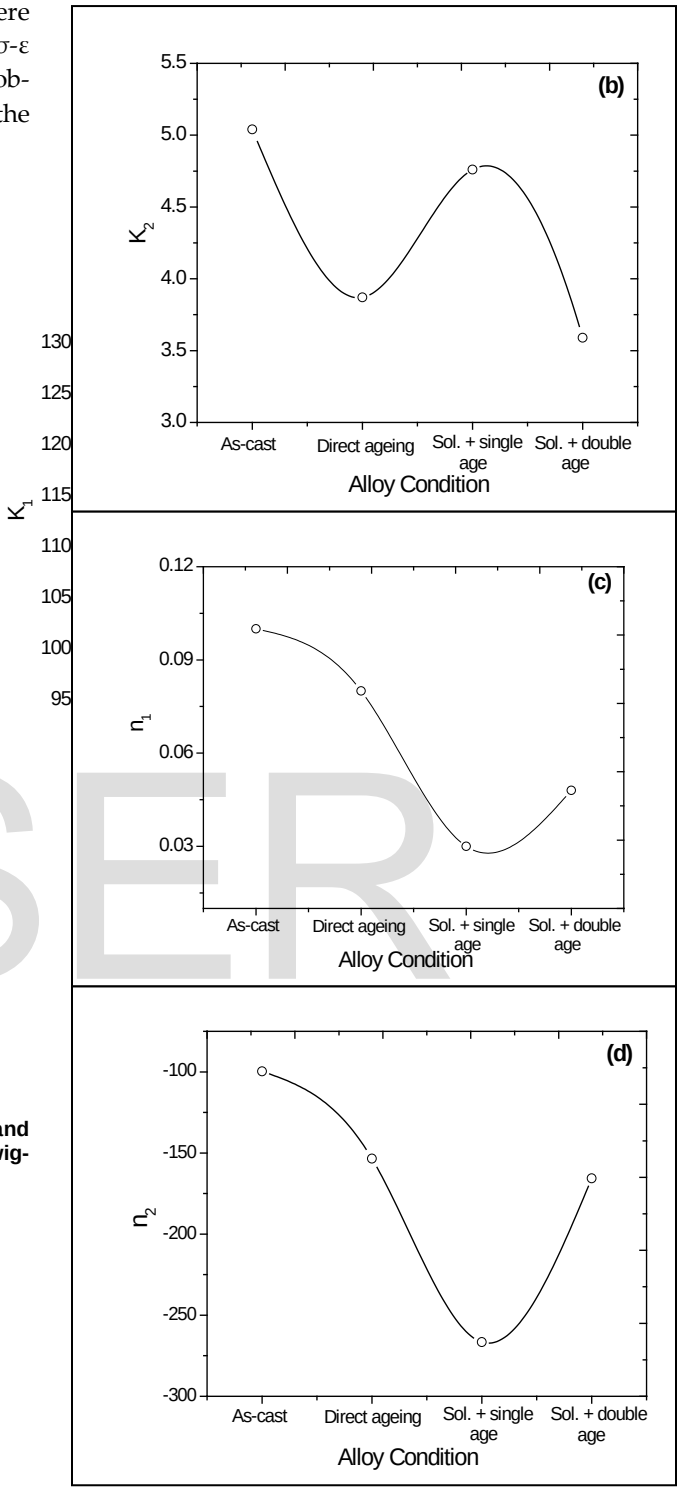

Fig. 4 Variation of parameters (a) K_1 (b) K_2 (c) n_1 and (d) n_2 with microstructural variation as obtained in as-cast and different heat treatment conditions of Supercast 247A alloy bars.

Figures 4 and 5 illustrate the effect of heat treatments on various flow parameters in the Ludwigson equation (Table 3). It is observed that the flow data of the aged alloys fitted according to Ludwigson model not only yield a unique set of flow pa-

rameters for each ageing condition but also exhibit a systematic trend. The parameters K_1, K_2 and ε_L first decrease by direct ageing of as-cast alloy, then increase with complete heat treatment involving single step aging and then again decrease with double ageing. On the other hand, n_1 and n_2 decreases up to single step aging then again slightly increase in the double ageing.

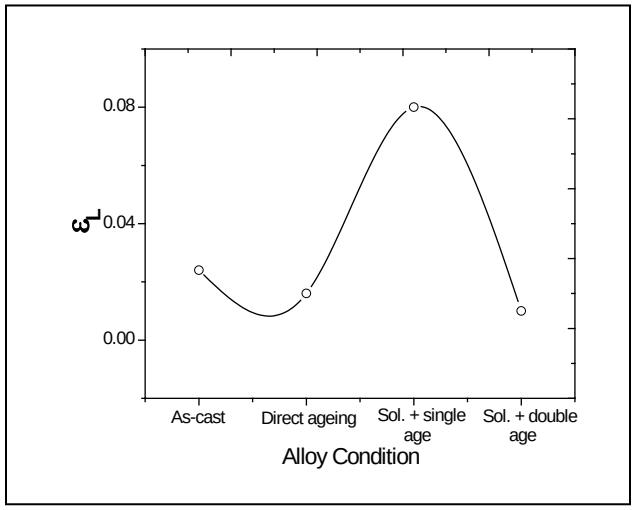

Fig. 5 Variation of transition strain, ε_L with different heat treatment and as cast conditions of Supercast 247A alloy bar at 298 K

The variation of K_1 and K_2 with heat treatment may be related to the combined resistance to motion of dislocations due to γ' precipitates and the dislocations substructure in the matrix. The initial decrease of K1 and K2 with direct ageing of the as-cast alloy can be attributed to the increase in γ' size. Subsequent increase in K_1 and K_2 (where e^{K_2} is equivalent to proportional limit as reported by Ludwigson [5]) following sol. + ageing at 870^{0}C is understandable as the latter results in precipitation of finer γ' precipitates in the matrix. Since double ageing involving ageing at 1080°C followed by 870°C results in coarsening of γ', the values of K_1 and K_2 again decrease. This behavior is consistent with variation of yield strength with different heat treatments as shown in Table 4.

Table 4. Tensile properties of Supercast 247A for different heat treatment conditions

Condition	0.2% YS (MPa)	UTS (MPa)	% Elongation	% Reduction in area
As cast	743	900	8.35	15.39
As cast + ageing	748	897	15.0	17.45
Solutioning + single ageing	881	911	5.6	13.71
Solutioning + double ageing	795	892	13.9	16.98

The parameters n_2 and ε_L (the transition strain) are inversely related to each other. The higher the negative value of n_2, the steeper the slope of the curve in the LSR and hence lower the value of ε_L i.e., the portion of the flow curve that can be represented by the Hollomon relation extends to lower strains. The reverse is true for lower negative values of n_2 i.e., ε_L increases as the absolute value of n_2 decreases. Since the parameters n_2 and ε_L (transition strain) are inversely related, the variation of these parameters with heat treatment condition has been observed to be in reverse. Thus, the Supercast 247A alloy in all conditions exhibit transient flow behavior at lower strains as can be seen from figure 2. A similar behavior exhibiting transient flow at low strains has also been reported earlier in a Fe-Ni-Cr-Al alloy strengthened by NiAl precipitates [6]. Furthermore, the flow data of the alloy in aged condition can also be described well using the Ludwigson model as evident from figure 3(a) (HSR) and figure 3(b) (LSR).

3.2 Strain Hardening Behaviour

Figure 6 illustrates variation of strain hardening rate, θ ($=d\sigma/d\varepsilon$) with plastic strain as well as stress, on log-log scale, for the alloy in different heat treatment conditions. These figures reveal that the alloy in all the conditions exhibit two regimes, rapid decrease of strain hardening rate in regime I followed by constant strain hardening rate in regime II.

The original C-J (Crussard and Jaoul [15]) plots for analysis of work hardening behavior is in terms of $\theta(=d\sigma/d\varepsilon)$ vs ε. However, subsequently, Reed-Hill and co-workers [16] pointed out that different regimes of work hardening represented by such plots were subjected to variations depending on the prior deformation history. They suggested that analysis in terms of θ versus σ plots is more appropriate as various regimes of such plots are not influenced by the prior deformation history. In the present study, both θ versus ε (Figs.6a) and θ versus σ (Fig.6b) plots, on log-log scale, have been examined. It is found that they are quite similar in the sense that both type of plots exhibit two distinct regimes of strain hardening and also, the level of strain hardening rates for different regimes are almost same in either case. They do not exhibit any deviations as reported by the earlier investigators. This behavior is, probably, due to the fact that the alloy used in the present study was in cast condition and not subjected to any prior deformation. Further, as evident from 6 (b), the curves for different heat treatment conditions are well separated, at least in regime I, when plotted in terms of θ vs. σ as compared to θ vs. ε plots (see data in Fig. 6).

As evident from Figs. 6 (a), the alloy in all conditions exhibit higher initial work hardening rates up to about 1%. This behavior may be explained based on the reported observations by Lewis MH and Martin JW [17] that for a given strain much

higher dislocation densities are generated in aged specimens as compared to precipitate –free matrix. This is because dispersed particles/ precipitates act as anchoring points for the multiplication of dislocations and also, their interfaces provide dislocation sources and thereby result in higher initial work hardening rates between solutionised and aged specimens. The decreasing strain hardening rate in regime I of aged specimens is similar to that of single phase alloys with high stacking fault energy, which is associated with dynamic recovery caused by cross slip and annihilation of screw components of dislocations. As the deformation precedes the decreasing strain hardening rate in regime II may be related to dynamic recovery caused by cross-slip and annihilation of screw components of dislocations of opposite sign from adjacent cells or tangled dislocation networks.

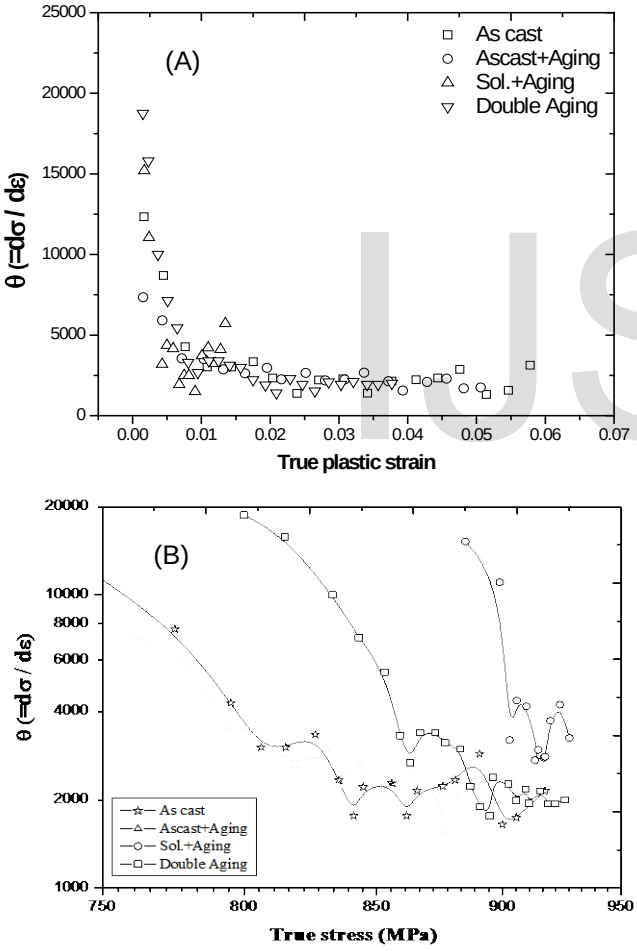

Fig. 6 Variation of strain hardening rate θ(=dσ/dε) with (a) Strain and (b) Stress in case of Supercast 247A alloy bar in As cast and different heat treatment conditions

As can be seen from Fig. 8b, the work hardening rate of the alloy progressively decreases as the size of γ' increases from sol. plus single aged condition through sol. plus double aged and as-cast conditions to as-cast plus direct aged condition. The alloy subjected to solution treatment followed by single step ageing at lower temperature (870 ºC) exhibits the highest work hardening rate as compared to all other conditions. This is because of the fact that the alloy with this heat treatment consists of finest and uniformly distributed γ'. On the other hand, the alloy subjected to double ageing, in spite of having coarsest secondary γ' structure compared to all the other conditions, exhibits the second highest strain hardening rate due to additional finer tertiary γ' structure resulting from second step ageing at lower temperature (i.e., at 870°C) i.e., bimodal γ' structure. These observations are consistent with the behaviour reported in case of an iron based (Fe-Ni-Cr-Al) [12] and nickel based superalloy (Inconel X 750) [13], where the work hardening rates are reported to be progressively decreasing with increase in precipitate size. In those alloys, such behavior is observed when the operating mechanism during deformation is Orowan bypassing as a result as of either precipitates are coherent but above certain size as in case of Inconel X 750 [13] or semicoherent as in case of a Fe-Ni-Cr-Al alloy [12]. In the light of these observations it may be appropriate to consider that Orowan bypass is the most probable deformation mechanism in the present alloy that contribute to decreasing strain hardening rate with increasing γ' size as observed in some of the earlier studies.

4 Conclusions

1. Experimental true stress – true strain data of the Supercast 247A alloy in all the conditions (As cast+ different heat treated conditions) have been analyzed using different flow relationships. Ludwigson relationship provides the best fit of the data for all the conditions except direct ageing, for direct ageing Ludwik relationship provides the best fit of the data.
2. The flow data of the alloy in all conditions, fitted according to Ludwigson model, not only yields a unique set of flow parameters for each aging condition but also exhibit a systematic trend. The parameters K_1, K_2 and ε_L first decrease by direct aging of as-cast alloy, then increase with complete heat treatment involving single step aging and then again decrease with double ageing. On the other hand n_1 and n_2 decreases up to single step aging then slightly increase in the double ageing.
3. The alloy in all heat treatment conditions exhibit two distinct stages of strain hardening with strain hardening rate decreasing rapidly in regime I, and remaining essentially constant in regime II. The strain hardening curves for different heat treatment conditions are well separated, at least in regime I, when plotted in terms of θ vs. σ as compared to θ vs. ε. The alloy subjected to solution treatment followed by single step ageing

exhibits highest work hardening rate of all the conditions studied because of its finer γ' size. The strain hardening rate of the alloy progressively decreases as the size of γ' increases from sol. plus single aged condition through solutionising plus double aged and as-cast conditions to as-cast plus direct aged condition.

ACKNOWLEDGMENT

The authors are grateful to Dr G. Malakondaiah, Distinguished Scientist and Director DMRL for his permission to use the facilities at DMRL. The authors would also like to thank Shri D.S.K. Murali for the help in the conduct of tensile testing at DMRL. Two of the authors (ChVSM and NEP) would like to thank Dr. K. Tamilmani, Distinguished Scientist and CE (Airworthiness), CEMILAC, for his kind support and encouragement.

REFERENCES

[1] J.H. Hollomon: Trans. AIME, 162 (1945) 268.
[2] P. Ludwick: Elements of the Technological Mechanic, Springer Publishers, Leipzig (1909) 32.
[3] E. Voce: Journal of Institute of Metals, 74 (1948) 537.
[4] H.W. Swift: Journal of Mech. Phys. Solids, 1 (1952) 1.
[5] D.G. Ludwickson: Metallurgical Transactions, 2 (1971) 2825.
[6] D.V.V. Satyanarayana, G. Malakondaiah, D.S. Sarma: Acta Materialia 452&453 (2004) 244.
[7] D.T. Llewelly: Materials Science and Technology 13 (1997) 389.
[8] I. Karaman, H. Schitoglu, Chumlyakovyi, H.J. Maier HJ: Journal of Metals 54 (2002) 31.
[9] J.R. Low, F. Garofalo: Proceedings of Society for Stress Analysis 4 (1947) 16.
[10] P.V. Sivaprasad, S. Venugopal, S. Venkatesan: Metallurgical and Materials Transactions 28A (1997) 171.
[11] P. Mullner, C. Salenthalar, P. Uggowitzer, M.O. Speidel: Material Science and Engineering 164A (1993) 164.
[12] D.V.V. Satyanarayana, K. Satya Prasad, G. Malakondaiah, D.S. Sarma: Materials Science and Technology 23 (2007) 79.
[13] J.A. Del Valle, A.C. Picasso, R. Romero: Acta Materialia 46 (1998) 981.
[14] K. Ankamma, D.V.V. Satyanarayana, Rajdeep Sarkar, G. Chandramohan Reddy, M. Komaraiah, N. Eswara Prasad: Materials Science and Technology 27 (2011) 1333.
[15] C. Crussard, B. Jaoul: Rev. Met. 8 (1950) 589.
[16] R.E. Reed-Hill, W.R. Cribb, S.N. Monteiro: Metallurgical Transactions 4 (1973) 2665.
[17] M.H. Lewis, J.W. Martin: Acta Metallurgica 11 (1963) 1207.